New High-Performance Piezoelectric: Ferroelectric Carbon-Boron Clathrate

Zhi Tan,[1] Hui Zhang,[2] Xiaojun Wu,[1] Jie Xing,[1,*] Qiming Zhang,[3] and Jianguo Zhu[1,†]
[1]College of Materials Science and Engineering, Sichuan University, Chengdu 610065, China
[2]School of Advanced Materials and Nanotechnology, Xidian University, Xi'an 710126, China
[3]Department of Physics, University of Texas at Arlington, Texas 76019, USA

(Received 8 November 2022; revised 26 March 2023; accepted 28 May 2023; published 13 June 2023)

High-performance piezoelectrics have been extensively reported with a typical perovskite structure, in which a huge breakthrough in piezoelectric constants is found to be more and more difficult. Hence, the development of materials beyond perovskite is a potential means of achieving lead-free and high piezoelectricity in next-generation piezoelectrics. Here, we demonstrate the possibility of developing high piezoelectricity in the nonperovskite carbon-boron clathrate with the composition of ScB_3C_3 using first-principles calculations. The robust and highly symmetric B-C cage with mobilizable Sc atom constructs a flat potential valley to connect the ferroelectric orthorhombic and rhombohedral structures, which allows an easy, continuous, and strong polarization rotation. By manipulating the cell parameter b, the potential energy surface can be further flattened to produce an extra-high shear piezoelectric constant d_{15} of 9424 pC/N. Our calculations also confirm the effectiveness of the partial chemical replacement of Sc by Y to form a morphotropic phase boundary in the clathrate. The significance of large polarization and high symmetric polyhedron structure is demonstrated for realizing strong polarization rotation, offering the universal physical principles to aid the search for new high-performance piezoelectrics. This work takes ScB_3C_3 as an example to exhibit the great potential for realizing high piezoelectricity in clathrate structure, which opens the door to developing next-generation lead-free piezoelectric applications.

DOI: 10.1103/PhysRevLett.130.246802

Perovskite ferroelectrics with the ABO_3 formula, such as lead zirconate titanate (PZT), barium titanate (BTO), and some Pb-based relaxors, are the widely used high-performance piezoelectric materials due to their outstanding electromechanical coupling property [1–7]. In the past two decades, the intrinsic origin of the high piezoelectricity near the morphotropic phase boundary (MPB) is identified from the ultrahigh shear piezoelectric constant, due to the strongly enhanced polarization rotation via a monoclinic bridge to connect the two distinct ferroelectric phases with flat potential energy surface [8–10]. The irreplaceable high piezoelectricity ensures the predominance of the materials with perovskite structure. However, a huge breakthrough in piezoelectric constants is found to be more and more difficult in recent years within these conventional perovskite materials. On the other hand, various new-type applications demand superior piezoelectricity, and to be lightweight and biofriendly [11]. Searching for new materials with high piezoelectricity beyond the perovskite structure is a feasible way for developing next-generation piezoelectrics.

To search the potential materials with high piezoelectricity, understanding the origin is crucial. Utilizing a simple transformation of the definition of piezoelectric constant d, the origin of the high shear piezoelectric constant can be well understood,

$$d_{\alpha j} = \left.\frac{\partial P_\alpha}{\partial \sigma_j}\right|_E = P\cos\theta_\alpha \left.\frac{\partial \theta_\alpha}{\partial \sigma_j}\right|_E = P\left.\frac{\partial \theta_\alpha}{\partial \sigma_j}\right|_E, \quad (1)$$

where P is the total polarization ($P_\alpha = P\sin\theta_\alpha$, only the pure polarization rotation behavior is considered), σ is stress, $\alpha = \{1,2,3\}$ in the Cartesian coordinate, $j = \{4,5,6\}$ in the Voigt notation, and θ is the polarization rotation angle. We consider the physical properties of the equilibrium state so that $\theta_\alpha = 0$. A schematic of the polarization rotation is shown in Fig. 1, suggesting that the lateral polarization can be greatly increased by a rotation of P. Equation (1) shows that the magnitude of P and the change rate of θ determine the shear piezoelectric

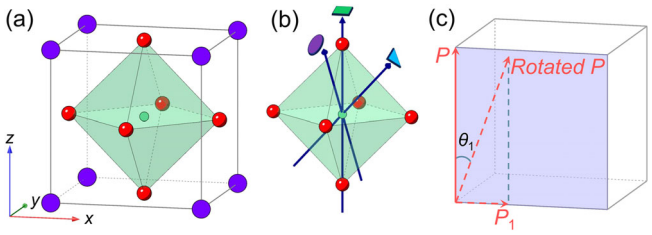

FIG. 1. (a) Typical perovskite-type structure. (b) Oxygen octahedron with high symmetry, the polarization rotation can be realized depending on the displacements of the B-site atom in the oxygen cage. (c) A schematic of polarization rotation on the (010) plane, where P_1 is the projection of rotated P in the x direction.

constant. The perovskite ferroelectrics usually have a large polarization and the change rate of θ can be greatly improved by forming MPB, in which the polarization rotation is mainly dependent on the easy and continuous change of displacement of the B site atom in the robust and highly symmetric oxygen cage. Despite that the intrinsic physical understanding of high piezoelectricity is clear, developing a material with high piezoelectricity beyond perovskite structure remains a decisive challenge because it is hard to realize easy, continuous, and strong polarization rotation in most ferroelectrics. For instance, $LiNbO_3$ [12] and Bi_2WO_6 [13] have enough large polarization, but their tilted polyhedron structures hinder the atomic movement to change the direction of polarization accompanied by steep potential energy surface [14].

To achieve high piezoelectricity, a material with a robust and highly symmetric polyhedron structure accompanied by multiple ferroelectric states and large polarization is crucial to allow the continuous movement of guest cations and thus realize the strong polarization rotation. Recently, a stable lightweight carbon-boron clathrate with the composition of SrB_3C_3 has been predicated and synthesized [15], which is composed of a strong sp^3-hybridized B-C framework with a high bulk modulus. The cubic SrB_3C_3 has a robust and large B-C cage, where the Sr locates at the center of the cage. Despite SrB_3C_3 being metallic, the replacement of Sr by Sc can form an insulating structure, which allows it to develop ferroelectricity depending on the Coulomb interaction between the off-centered Sc^{3+} cation and the negatively charged B-C cage [16]. We noted that the ferroelectric ScB_3C_3 has a huge spontaneous polarization, and the B-C framework exhibits a highly symmetric truncated octahedron clathrate. This truncated octahedron clathrate allows Sc to be displaced towards the center of the common edge of B-C hexagon or centroid of B-C hexagon or square, forming $\langle 110\rangle_{pc}$, $\langle 100\rangle_{pc}$, or $\langle 111\rangle_{pc}$ polarization to produce three distinct ferroelectric phases [16], which is similar to the perovskite case. The results show that it is possible to realize the strong polarization rotation by controlling the continuous displacement of Sc in the B-C cage. The clathrate ferroelectrics can be regarded as a new class of ideal high-performance piezoelectric materials.

This Letter takes ScB_3C_3 as an example to exhibit the great potential for realizing high piezoelectricity in a nonperovskite clathrate structure. The easy, continuous, and strong polarization rotation can be realized in the highly symmetric truncated octahedron B-C clathrate with a smaller Sc atom. By inducing epitaxial strain or homovalent substitution, we anticipate that the potential energy landscape can be further flattened, resulting in the formation of MPB and concomitant high piezoelectricity. Our findings highlight the feasibility of developing high piezoelectricity in clathrate ferroelectrics and provide a theoretical foundation for the pursuit of high-performance piezoelectric materials. These results are expected to inspire the creation of next-generation, nonperovskite, high-performance piezoelectric applications.

The first-principle calculations in the present work are carried out using the Vienna *ab initio* simulation package (VASP) based on density functional theory (DFT) [17,18]. The strongly constrained and appropriately normed (SCAN) meta-GGA functional is used to process the exchange-correlation functional [19], which shows an excellent ability to capture ferroelectric distortion [20]. The projector augmented-wave (PAW) potential is employed to describe the electron-ion potential [21]. The Sc $3s^23p^63d^14s^2$, Y $4s^24p^64d^15s^2$, B $2s^22p^1$, and C $2s^22p^2$ states are treated as valence electrons for calculations. The wave function is represented as a plane wave expansion that is truncated at a cutoff energy of 520 eV. The Kohn-Sham orbitals are updated in the self-consistency cycle until an energy convergence of 10^{-6} eV is obtained, and the geometry optimizations are completed when the residual force of each atom is less than 0.001 eV/Å. To overcome the underestimate of band gaps, we adopted the PBE0 hybrid functional [22] to obtain the macroscopic polarization of ScB_3C_3 using the so-called modern theory of polarization [23–25]. We use a $2\times2\times2$ supercell to compare the energies of orthorhombic and rhombohedral phase in the partial Y-replaced ScB_3C_3, where the Y and Sc atoms are randomly placed at the center of B-C framework by the special quasi-random structure (SQS) approach [26], in which the convergence criteria for the residual force of each atom loosen to 0.01 eV/Å. The on-the-fly machine learning force fields (MLFF) [27,28] are trained in a $2\times2\times2$ supercell to conduct the *ab initio* molecular dynamics (MD). For the training, the simulations are executed in the *NPT* ensemble for 50 ps using the time step of 1 fs at 50, 150, 300, 500, and 800 K, respectively. Based on the generated MLFF, heating MD simulations with a heating rate of 2 K/ps are carried out on the $4\times4\times4$ supercell. The total MD simulation times of 30 ps are used to obtain the dynamic structures at constant temperatures of 100, 250, and 500 K, respectively.

The cubic ScB_3C_3 are shown in Fig. 2(a) with the space group $Pm\bar{3}n$ (No. 223), containing 2 Sc, 6 B, and 6 C atoms. In this structure, the Sc is located at the center of a truncated octahedron clathrate, which is composed of a strong sp^3-hybridized B-C framework [16]. The high symmetry of truncated octahedron clathrate allows many equivalent Sc displacements, such as $\langle 001\rangle_{pc}$, $\langle 011\rangle_{pc}$, and $\langle 111\rangle_{pc}$, forming $P4_2mc$, $Ama2$, and $R3c$ phases, respectively. Zhu *et al.* have demonstrated the ferroelectricity of ScB_3C_3 using PBE exchange [16], suggesting the orthorhombic phase is the ground state. We revisit this result by employing a more powerful SCAN meta-GGA. By comparing the energy difference of various phases, the orthorhombic phase with $Ama2$ space group (No. 40) is confirmed as the ground state again [29]. The curve of

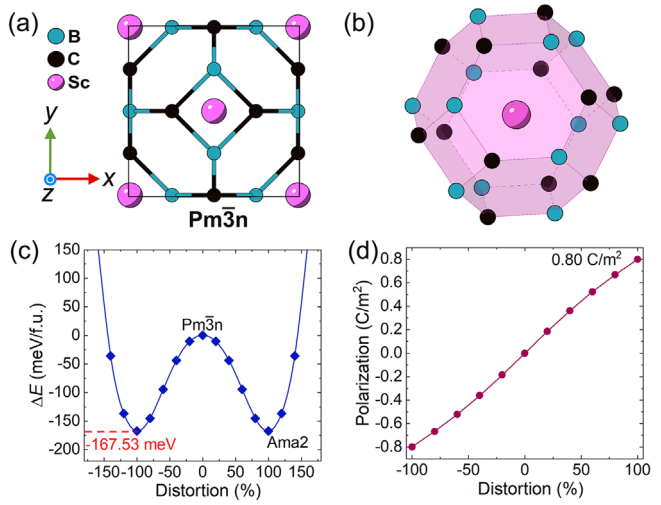

FIG. 2. (a) Structure of cubic ScB_3C_3. (b) High symmetry of carbon-boron clathrate. (c) Total energies vs full-mode distortion of orthorhombic ferroelectric phase. (d) Polarization vs the distortion. Note that only one branch of polarization quantum is chosen.

energy vs. the full distortion associated with the $Ama2$ is plotted in Fig. 2(c), which presents a typical double well as a ferroelectric. It must be noted that the Sc atoms are displaced along $[011]_{pc}$ direction, closing to the common edges of the B-C hexagon. We check the electron localization function for the orthorhombic ScB_3C_3, and the strong covalent bonding between B and C atoms is revealed [29], which is the cornerstone for the construction of the substantial truncated octahedral cage. While a large displacement of Sc can be found in the B-C cage in Fig. S1 [29], which is the main origin of the high polarization. By employing the modern theory of polarization, a branch of polarization quantum is plotted in Fig. 2(d) and a high polarization of 0.80 C/m^2 is identified in orthorhombic ScB_3C_3.

We employ the energy-strain method and polarization-strain method to compute the elastic stiffness tensor and piezoelectric stress tensor of orthorhombic ScB_3C_3, as shown in Table I. We noted the ScB_3C_3 possesses very

TABLE I. Calculated elastic stiffness constants c_{ij}, piezoelectric stress constants $e_{\alpha j}$, and piezoelectric strain constants $d_{\alpha j}$ of orthorhombic ScB_3C_3. c_{ij}, $e_{\alpha j}$, and $d_{\alpha j}$ are in GPa, C/m^2, and pC/N, respectively.

c_{11}	c_{22}	c_{33}	c_{12}	c_{13}	c_{23}	c_{44}	c_{55}	c_{66}
373	404	383	198	162	92.9	37.2	43.8	128

e_{31}	e_{32}	e_{33}	e_{24}	e_{15}
0.67	0.41	3.00	−1.37	10.67

d_{31}	d_{32}	d_{33}	d_{24}	d_{15}
−1.96	−0.02	8.67	−36.8	244

hard longitudinal and transverse elastic constants, where c_{33} is almost several times larger than conventional perovskite ferroelectrics, such as $PbTiO_3$ [30] and $BaTiO_3$ [31]. The high hardness goes against the high piezoelectricity. Fortunately, the shear elastic stiffness constants associated with the c direction are low, which allows generating the shear deformation easily accompanied by strong polarization rotation. The result shows only 8.67 pC/N of d_{33} can be obtained due to the stiff elastic constant, but 244 pC/N of d_{15} is achieved by the combination of low c_{55} and high e_{15} according to $d_{15} = e_{15}/c_{55}$, which is comparable with most of conventional perovskite piezoelectric materials [32]. In addition, we noted an abnormal negative d_{24}, which means the polarization rotation turns to the negative y direction when a positive shear strain η_4 is applied on the cell.

To understand the origin of negative e_{24} and high e_{15}, the $e_{\alpha j}$ is decomposed as

$$e_{\alpha j} = e^f_{\alpha j} + \sum_k \frac{ec}{\Omega} Z^*_{\alpha\alpha} \frac{u_\alpha}{\eta_j}, \tag{2}$$

where the e^f is the frozen-ion term with the fixed internal atomic coordinate (u). Here, k runs over the atoms in the unit cell of volume Ω, e is the electron charge, c is the lattice constant along the polar axis, and Z_{ii} is the Born effective charge. The computed e^f_{24} is −1.636 C/m^2, being attributed to the change of charge center of Sc to the positive y direction when the η_4 is applied, as shown in Figs. S4 and S5 [29]. Meanwhile, the $\partial u_2/\partial\eta_4$ term of Sc along the y direction is very small under the η_4 [29], finally giving rise to negative e_{24}.

The e^f_{15} is still negative, however, the $\partial u_1/\partial\eta_5$ term is quite strong, dominating the total piezoelectric response of 15 mode [29]. By decomposing the relaxed-ion term of three kinds of atoms, we noted the high piezoelectricity mainly comes from the change of the internal coordinate of Sc, having 81.4% contribution, while the B and C atoms have, respectively, −2.5% and 21.1% contribution. The $\partial u_1/\partial\eta_5$ terms of Sc, B, and C atoms suggest that the carbon-boron clathrate constructs a large and substantial frame, which allows the smaller Sc atom in the B-C cage to produce a significant change of displacement depending on the external field, which is essential for a strong polarization rotation. We computed the polarization rotation angle as a function of shear strain η_5, as shown in Fig. S6 [29], a high rotation angle of 26.04° is obtained at $\eta_5 = 3\%$, which is fairly strong and almost realizing complete rotation of 35.26° between $[111]_{pc}$ to $[011]_{pc}$. Our calculations confirm that continuous and strong rotation is possible under the shear strain η_5, suggesting the high piezoelectricity maybe stems from the low energy difference (4.3 meV/f.u.) between rhombohedral and orthorhombic phases.

To further understand the nature of shear piezoelectricity, the investigation of the potential energy surface (PES) is needed. With the cubic structures as a reference, we use the

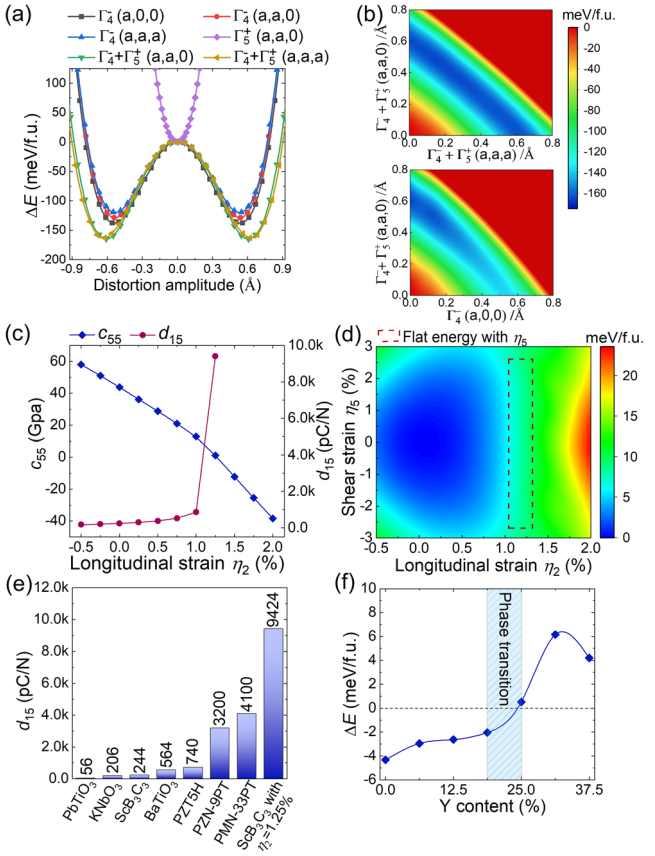

FIG. 3. (a) Potential energy as a function of the amplitude of distortion mode. (b) PES as a function of $\Gamma_4^- + \Gamma_5^+$ (a, a, 0) and $\Gamma_4^- + \Gamma_5^+$ (a, a, a), as well as $\Gamma_4^- + \Gamma_5^+$ (a, a, 0) and Γ_4^- (a, 0, 0). (c) c_{55} and d_{33} as a function of longitudinal strain η_2. The negative c_{55} indicates the phase transition. (d) PES as a function of η_2 and η_5. (e) d_{15} of ScB_3C_3 compared with other inorganic perovskite ferroelectrics [35–39]. (e) Difference of total energy between orthorhombic and rhombohedral phases as a function of Y content.

crystallographic tool AMPLIMODE [33,34] to decompose the distortions of ferroelectric ScB_3C_3. Two major distortions, Γ_5^+ and Γ_4^-, play important roles for the formation of the orthorhombic and rhombohedral phases, and only one major Γ_4^- distortion is confirmed in the tetragonal phase. We found the Γ_4^- distortion captures exceed 97% of total distortion in the three ferroelectric phases. However, Fig. 3(a) shows that Γ_4^- (a, 0, 0) results in the lowest potential in single-mode distortion, suggesting another mode plays a key role to stabilize (a, a, 0) polarization. Combining the Γ_4^- (a, a, 0) and Γ_5^+ (a, a, 0) distortions, the potential is greatly decreased to −165.5 meV, while the single Γ_5^+ (a, a, 0) mode just shows a single-well curve. The results demonstrate that the coupling of Γ_4^- and Γ_5^+ is crucial to lowering the potential for promoting the formation of the orthorhombic ground state. Two-dimensional PES is computed by changing the distortion amplitude, as shown in Fig. 3(b). The structure without any distortion always keeps a high energy barrier, and the energy of these (a, a, 0) and (a, a, a) minima relative to the cubic structure is around −165 meV/f.u., seeming it appears unlikely to directly crossing the barrier. However, a rift valley with a flat bottom can be found to connect the $\Gamma_4^- + \Gamma_5^+$ (a, a, 0) and $\Gamma_4^- + \Gamma_5^+$ (a, a, a) modes, which is conducive to facilitating polarization rotation between orthorhombic and rhombohedral ferroelectric phases. A similar situation is found in the PES involved $\Gamma_4^- + \Gamma_5^+$ (a, a, 0) and Γ_4^- (a, 0, 0) modes, but the bottom of the rift valley is steeper than that of above.

Figure 3(b) indicates that the high d_{15} is closely related to the phase transition from $Ama2$ to $R3c$ via the potential valley, and we found that the PES can be further flattened by manipulating the lattice parameter b. With the increased strain η_2, the potential with respect to η_5 is gradually flatted, as shown in Fig. 3(d). Finally, the second derivative turns negative at $\eta_2 \geq 1.5\%$, indicating the dynamically unstable. In this process, the elastic stiffness constant c_{55} gradually decreases, and a very small value of 1.18 Gpa can be obtained at $\eta_2 = 1.25\%$, where the e_{15} is 11.12 C/m^2. The strong polarization rotation and soft shear deformation boost a very high d_{15} of 9424 pC/N, which even exceeds the relaxor-ferroelectrics, such as PMN-PT and PZN-PT [37,38]. The modulation of positive η_2 suggests that the decrease of b/c is conducive to inducing phase transition from orthorhombic to rhombohedral phases. We also consider a chemical replacement to construct the MPB. The partial substitution of Sc using homovalent Y is carried out to study the phase transition, where the YB_3C_3 has been confirmed as a dynamically stable compound [40]. As illustrated in Fig. 3(f), the ground state transforms into the rhombohedral phase upon reaching a Y content of 25%, thereby implying that chemical substitution represents an efficacious strategy for establishing MPB and offering a more promising pathway for experimentally realizing high piezoelectricity. All the results suggest that the carbon-boron clathrate structure has great potential to be used for high-performance piezoelectric applications.

To explore the phase transition order, the on-the-fly MLFF based on the first-principle calculations are carried out to perform the MD simulations. Figure 4(a) demonstrates the temperature-dependent polarization evolution of ScB_3C_3 in a $4 \times 4 \times 4$ supercell (896 atoms). Two abrupt changes can be found at 160 and 340 K, respectively, suggesting the phase transitions. Combined the energy difference between phases and temperature-dependent lattice parameters (see Fig. S9 [29]), it has been determined that the orthorhombic phase undergoes a transition to the rhombohedral phase at 160 K, followed by a subsequent loss of ferroelectricity at 340 K. The thermotropic phase transition is like the situation of $BaTiO_3$, which can be expected to be shifted to room temperature for realizing high piezoelectricity. We also explore the spatial distribution of Sc displacement relative to carbon-boron

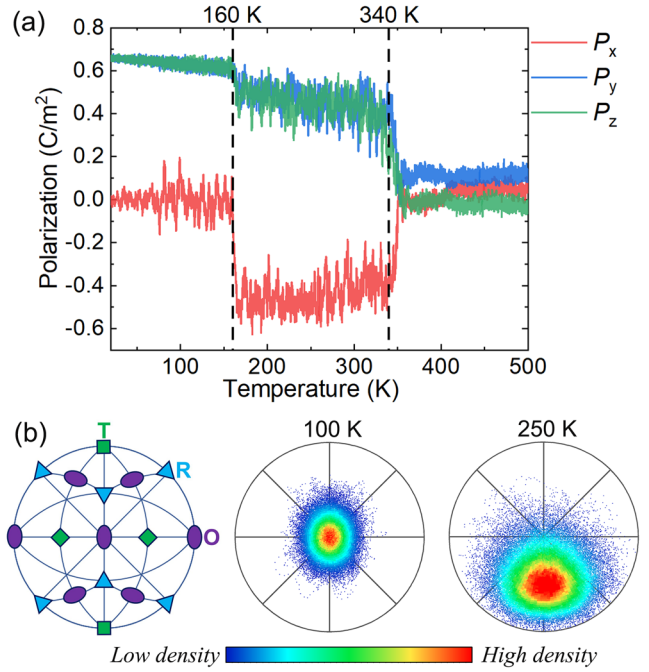

FIG. 4. (a) Temperature-dependent polarization in ScB_3C_3. (b) $[011]_{pc}$ stereographs of the direction of polar displacement of Sc in carbon-boron clathrate. The colors exhibit the density distribution around each point on the graph.

clathrate at a different phase, which is the major origin of ferroelectricity. As shown in Fig. 4(b), the distribution of Sc at 100 K is elliptic viewed from the $[011]_{pc}$ direction, and the semimajor axis points to the $[111]_{pc}$ direction attributed to the low potential surface along the direction. The area of distribution is significantly enlarged at 250 K, and the shape is like a regular triangle, which is extended along the adjacent $\langle 110\rangle_{pc}$ direction. All the results agree with the fact that the potential valley with a flat can connect the orthorhombic and rhombohedral phases to promote polarization rotation. Moreover, the distribution of Sc displacement is closely related to polarization instability accompanied by high piezoelectricity [41].

In summary, the significance of the highly symmetric polyhedron structure accompanied by multiple ferroelectric states and large polarization is shown for realizing high piezoelectricity. We demonstrate the principle to confirm the high piezoelectricity in a recently found nonperovskite carbon-boron clathrate with the composition of ScB_3C_3 using the first-principle calculations. A rift valley of potential energy surface with a flat bottom constructs the bridge to connect the $Ama2$ and $R3c$ phases, helping to realize strong polarization rotation in ScB_3C_3. We predicate that the potential energy surface can be further flattened under the strain $\eta_2 = 1.25\%$, boosting extremely enhanced $d_{15} \sim 9424$ pC/N. Our calculations also confirm that partial chemical replacement of Sc by Y is another experimentally feasible method to facilitate the formation of MPB. The MLFF-based MD simulations suggest a thermotropic ferroelectric phase transition from orthorhombic to rhombohedral phase around 160 K. This work will inspire research of the new-type piezoelectric materials beyond perovskite structure, which allows the possibility to achieve high piezoelectricity in next-generation lead-free high-performance piezoelectrics.

This work is supported by the National Natural Science Foundation of China (No. 52032007, No. 12004267, No. 52202294), the Key-Area Research and Development Program of Guangdong Province (No. 2020B0109380001), the Fundamental Research Funds for the Central Universities of China (No. 2021SCU12058, No. XJS221403), the Natural Science Foundation of Sichuan Province (No. 2022NSFSC0376).

*Corresponding author.
xingjie@scu.edu.cn
†Corresponding author.
nic0400@scu.edu.cn

[1] K. Uchino, Sci. Technol. Adv. Mater. **16**, 046001 (2015).
[2] K. Uchino, *Piezoelectric Actuators and Ultrasonic Motors* (Kluwer Academic Publishers, Boston, 1996).
[3] M. A. Akbas and P. K. Davies, J. Am. Ceram. Soc. **81**, 670 (1998).
[4] W. Liu and X. Ren, Phys. Rev. Lett. **103**, 257602 (2009).
[5] N. Zhang, H. Yokota, A. M. Glazer, Z. Ren, D. A. Keen, D. S. Keeble, P. A. Thomas, and Z.-G. Ye, Nat. Commun. **5**, 1 (2014).
[6] I. Grinberg, Y. H. Shin, and A. M. Rappe, Phys. Rev. Lett. **103**, 197601 (2009).
[7] F. Li, M. J. Cabral, B. Xu, Z. Cheng, E. C. Dickey, J. M. LeBeau, J. Wang, J. Luo, S. Taylor, W. Hackenberger, L. Bellaiche, Z. Xu, L.-Q. Chen, T. R. Shrout, and S. Zhang, Science **364**, 264 (2019).
[8] D. Vanderbilt and M. H. Cohen, Phys. Rev. B **63**, 094108 (2001).
[9] B. Noheda, D. E. Cox, G. Shirane, J. A. Gonzalo, L. E. Cross, and S.-E. Park, Appl. Phys. Lett. **74**, 2059 (1999).
[10] R. Guo, L. E. Cross, S.-E. Park, B. Noheda, D. E. Cox, and G. Shirane, Phys. Rev. Lett. **84**, 5423 (2000).
[11] Y.-M. You, W.-Q. Liao, D. Zhao, H.-Y. Ye, Y. Zhang, Q. Zhou, X. Niu, J. Wang, P.-F. Li, D.-W. Fu, Z. Wang, S. Gao, K. Yang, J.-M. Liu, J. Li, Y. Yan, and R.-G. Xiong, Science **357**, 306 (2017).
[12] R. I. Shostak, S. V. Yevdokimov, and A. V. Yatsenko, Crystallogr. Rep. (Transl. Kristallografiya) **54**, 492 (2009).
[13] Z. Tan, J. Xi, J. Xing, B Wu, Q. Zhang, Q. Chen, and J. Zhu, J. Eur. Ceram. Soc. **42**, 3865 (2022).
[14] K. Yan, S. Ren, M. Fang, and X. Ren, Acta Mater. **134**, 195 (2017).
[15] L. Zhu, G. M. Borstad, H. Liu, P. A. Guńka, M. Guerette, J.-A. Dolyniuk, Y. Meng, E. Greenberg, V. B. Prakapenka, B. L. Chaloux, A. Epshteyn, R. E. Cohen, and T. A. Strobel, Sci. Adv. **6**, eaay8361 (2020).
[16] L. Zhu L, T. A. Strobel, and R. E. Cohen, Phys. Rev. Lett. **125**, 127601 (2020).

[17] G. Kresse and J. Hafner, Phys. Rev. B **49**, 14251 (1994).
[18] G. Kresse and J. Furthmüller, Phys. Rev. B **54**, 11169 (1996).
[19] J. Sun, A. Ruzsinszky, and J. P. Perdew, Phys. Rev. Lett. **115**, 036402 (2015).
[20] Y. Zhang, J. Sun, J. P. Perdew, and X. Wu, Phys. Rev. B **96**, 035143 (2017).
[21] P. E. Blöchl, Phys. Rev. B **50**, 17953 (1994).
[22] J. P. Perdew, M. Ernzerhof, and K. Burke, J. Chem. Phys. **105**, 9982 (1996).
[23] R. D. King-Smith and D. Vanderbilt, Phys. Rev. B **47**, R1651 (1993).
[24] R. Resta, Eur. Phys. Lett. **22**, 133 (1993).
[25] D. Vanderbilt and R. D. King-Smith, Phys. Rev. B **48**, 4442 (1993).
[26] A. van de Walle, P. Tiwary, M. de Jong, D. Olmsted, M. Asta, A. Dick, D. Shin, Y. Wang, L.-Q. Chen, and Z.-K. Liu, CALPHAD: Comput. Coupling Phase Diagrams Thermochem. **42**, 13 (2013).
[27] R. Jinnouchi, F. Karsai, and G. Kresse, Phys. Rev. B, **100**, 014105 (2019).
[28] R. Jinnouchi, J. Lahnsteiner, F. Karsai, G. Kresse, and M. Bokdam, Phys. Rev. Lett. **122**, 225701 (2019).
[29] See Supplemental Material at http://link.aps.org/supplemental/10.1103/PhysRevLett.130.246802 for detailed crystal structure information, energy difference with respect to cubic phase, distortion matrix used in energy-strain method, electron localization function, electronic charge density, polarization, and internal coordinate changes under applying the strain, charge density difference for interpretation of negative d_{24}, rotation angle as a function of η_5, orientation dependences of effective piezoelectric constant d_{33}, pair correlation functions at 100, 250, and 500 K, respectively, and the lattice parameters changes vs temperature.
[30] Z. Wu and R. E. Cohen, Phys. Rev. Lett. **95**, 037601 (2005).
[31] X. Meng, X. Wen, and G. Qin, Comput. Mater. Sci. **49**, S372 (2010).
[32] M. Davis, M. Budimir, D. Damjanovic, and N. Setter, J. Appl. Phys. **101**, 054112 (2007).
[33] D. Orobengoa, C. Capillas, M. I. Aroyo, and J. M. Perez-Mato, J. Appl. Crystallogr. **42**, 820 (2009).
[34] J. M. Perez-Mato, D. Orobengoa, and M. I. Aroyo, Acta Crystallogr. Sect. A **66**, 558 (2010).
[35] M. Zgonik, R. Schlesser, I. Biaggio, E. Voit, J. Tscherry, and P. Gýnter, J. Appl. Phys. **74**, 1287 (1993).
[36] M. Zgonik, P. Bernasconi, M. Duelli, R. Schlesser, P. Günter, M. H. Garrett, D. Rytz, Y. Zhu, and X. Wu, Phys. Rev. B **50**, 5941 (1994).
[37] H. Dammak, A.-E. Renault, P. Gaucher, M. P. Thi, and G. Calvarin, Jpn. J. Appl. Phys. **10**, 6477 (2003).
[38] R. Zhang and W. Cao, Appl. Phys. Lett. **85**, 6380 (2004).
[39] M. J. Haun, E. Furman, S. J. Jang, H. A. McKinstry, and L. E. Cross, J. Appl. Phys. **62**, 3331 (1987).
[40] S. D. Cataldo, S. Qulaghasi, G. B. Bachelet, and L. Boeri, Phys. Rev. B **105**, 064516 (2022).
[41] K. Datta, I. Margaritescu, D. A. Keen, and B. Mihailova, Phys. Rev. Lett. **121**, 137602 (2018).